Enhanced Tensile Performance of Laser Additive Manufactured Tix-AlCoCrFeNi2.1 High Entropy Alloys

Yixuan Sun[1], Chunjin Wang*, Xingdong Dan, Chuanxi Ren, Xiaoliang Liang, Chi Fai Cheung, Zibin Chen*

1State Key Laboratory of Ultra-precision Machining Technology, Department of Industrial and Systems Engineering, The Hong Kong Polytechnic University, Hung Hom, Hong Kong, China
Corresponding Author / Email: chunjin.wang@polyu.edu.hk, TEL: +852-3400-3190, FAX: +852−2764−7657

KEYWORDS: Laser Additive Manufacturing, Mechanical Performance, High Entropy Alloys

TixAlCoCrFeNi2.1 (where x = 0, 0.15, 0.3) eutectic high-entropy alloys (EHEAs) were synthesized using the Laser Energy Net Shaping (LENS) technique. The effects of minor Ti additions on the microstructural characteristics were examined utilizing scanning electron microscopy (SEM), accompanied by tensile testing to assess mechanical properties. The findings demonstrate a morphological transition in the microstructures from lamellar to petal-like configurations as distinct Ti contents are incorporated. Concurrently, an augmentation in Ti content leads to a progressive enhancement in ultimate tensile strength (UTS), albeit with a marginal reduction in elongation. Notably, the Ti0.15AlCoCrFeNi2.1 alloy produced through LENS fabrication exhibits a favorable synergy between UTS (1420 MPa) and satisfactory ductility (8%), thereby providing valuable insights for the optimization of high-entropy alloy design.

1. Introduction

Throughout human history, metallic materials have held essential roles in both industrial production and daily life, evolving from the Stone Age to the Iron Age [1]. As industrial demands increase, there is a growing focus on enhancing the strength and toughness of metallic materials, which often exhibit a trade-off relationship [2]. Researchers have primarily explored alloying and structural methods over the past three decades to mitigate this trade-off and improve material performance. Alloying introduces defects like line defects, dislocations, and grain boundaries, while structuring involves introducing alloying elements to obstruct grain dislocations. In 2004, the novel concept of high-entropy alloys (HEAs) emerged, blending four or more elements in nearly equal proportions to create a solid solution [3]. HEAs exhibit four core effects - high entropy, hysteretic diffusion, lattice distortion, and cocktail effects-yielding desirable properties such as wear resistance, high strength, high-temperature softening, hardness, and corrosion resistance. This has led to the exploration of eutectic high-entropy alloys (EHEAs), which combine the benefits of eutectic and high-entropy concepts, resulting in a synergistic balance of strength and ductility [4]. Laser additive manufacturing (LAM) has gained attention as a method for fabricating high-performance metallic parts with precise geometries [5]. By altering the elements and proportions of HEAs, LAM can modify their microstructure and properties, presenting the potential for large-scale industrial applications. Recent developments have shifted the strength-toughness curve of high-entropy alloys, and questions remain regarding HEAs and LAM: optimizing parameters for forming HEAs, addressing challenges in processing and fabrication due to their unique characteristics, and understanding the fundamental principles governing their properties.

This study delves into the fundamental principles governing properties of HEAs, encompassing the impacts of composition, crystal structure, and processing on mechanical attributes. It investigates phase formation in EHEAs and microstructural evolution. The objective is to design and optimize HEA systems that strike a balance between strength and plasticity, considering the diverse composition possibilities HEAs offer. This research paper undertakes optimization of LAM process parameters, investigating microstructure evolution laws of LAM-formed HEA and discerning related mechanisms. The paper proceeds to refine dual-phase high-entropy alloy compositions and control their structure. Further studies encompass room temperature mechanical properties of LAM-formed dual-phase high alloys, unraveling plastic deformation mechanisms, and quantitatively evaluating tensile properties.

2. Material Method

Gas-atomized AlCoCrFeNi2.1 pre-alloyed spherical powder (45-105 μm) and high-purity Ti metal powder (> 99.9 wt%, 45-105 μm) were thoroughly mixed using a 3D shaking mixer for 2 hours. Morphology and structure were analyzed through optical microscopy (ZEEISS Axiolab 5) and scanning electron microscopy (SEM) (VEGA 3, TESCAN), confirming the near-spherical shape of the blended powders. Laser Energy Net Shaping (LENS) experiments utilized a stainless-steel substrate, chosen for enhanced bonding and reduced energy consumption. Specimens (35 × 10 × 5 mm) were fabricated using a commercial LENS machine (MR-7, Optomec). The LENS process occurred under an argon atmosphere (<30 ppm residual oxygen), ensuring process integrity and minimal contamination, as shown in Figure 1(a). A consistent 90° rotation between successive layers was employed (Figure 1(b)).

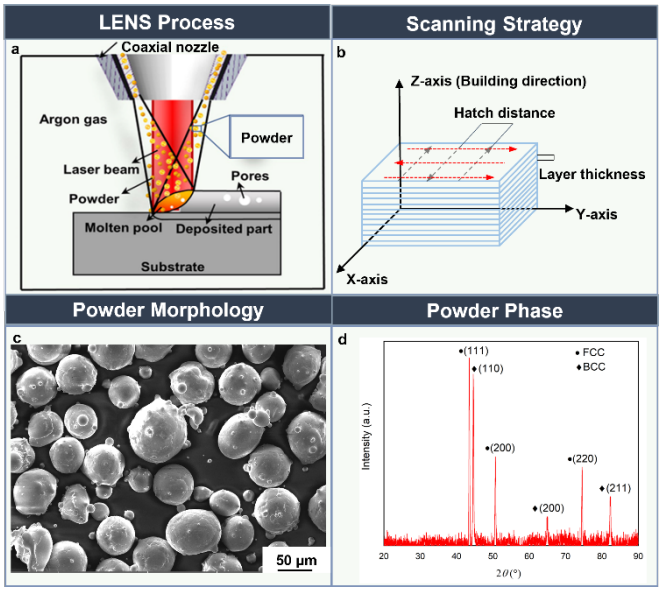

Fig. 1 The illustration of the LENS equipment (a) and laser scanning strategy (b), SEM images showing the powder morphology of EHEA (a), and the XRD patterns of the raw EHEA pre-alloy powder phase (d).

To assess EHEAs' printability, a comprehensive variation of process parameters was systematically executed. Archimedes' principle determined the relative density of each sample. Rigaku Smartlab-9 kW X-ray diffractometry (Tokyo, Japan) employed Cu-K α radiation to analyze phase composition in EHEA-Tix. Dog-bone-shaped tensile test samples were wiring electro-discharge machined, followed by grinding and polishing. Tensile tests, parallel to the build direction, utilized a Struers Duramin-40 testing machine at a strain rate of 1×10^{-3} s^{-1}, with each test repeated thrice for precision. Microhardness was measured using a Zwick Roell Z020 TEW Microhardness tester. Samples were prepared under various laser powers (150 W, 240 W, 300 W, 350 W) and scanning speeds (6 mm/s, 8 mm/s). The utilization of *LED* facilitated a comparative analysis of different parameter sets, serving as an indicator of densification behavior resulting from the varied processing conditions, The densification is defined by the input laser energy density (P_{laser}), the laser scan speed (v_{scan}) [6]:

$$LED = \frac{P_{laser}}{v_{scan}} \quad (1)$$

3. Results and discussions

Fig. 2 shows relative density as a function of *LED*. At a relatively low LED of 25 J/mm and of 40 J/mm, the sample had unmelted powders (Fig. 2b) and a large number of micrometer-sized balls with diameters of about 50 μm were formed along the solidified liquid front (Fig. 2c). Nevertheless, at a reasonable intermediate *LED* of 50 J/mm, a clear and regular liquid solidification front free of any clusters of balls was observed, leading to the formation of stable and continuous deposited layers. With an increasing *LED* up to 58 J/mm, the liquid solidification front started to become irregular and considerably disordered, resulting in the formation of large-sized gaseous balls. Most likely, the too-high *LED* leads to the evolution of a turbulent liquid solidification front and subsequent significant formation of gaseous pores.

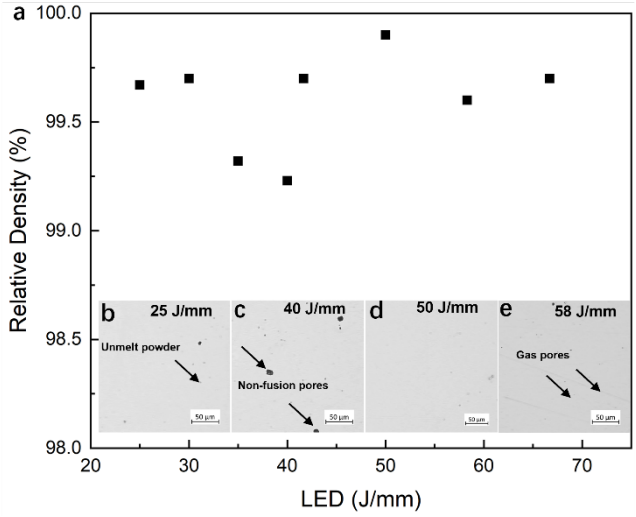

Fig. 2 Relative density as a function of *LED* (a); OM images showing the formability in EHEA, 25 J/mm (b), 40 J/mm (c), 50 J/mm (d) and 58 J/mm (e).

The optical microscope in Figure 3 depicts the microstructural characteristics of EHEA, Ti0.15-EHEA, and Ti0.3-EHEA alloys. The EHEA alloy reveals a classical lamellar eutectic microstructure comprising two phases. The lamellar spacing between these phases measures approximately 2 μm, indicating a significant reduction compared to the eutectic spacing observed in the as-cast samples, which is approximately 3.5 μm [7]. The utilization of LENS results in substantially higher cooling rates compared to conventional fabrication methods, thereby facilitating the refinement of the solidification microstructure. Upon incrementing the Ti content, a microstructure evolution is noted, the microstructural morphology undergoes a transition from lamellae to petal-like configurations, mirroring the evolution of Ti content.

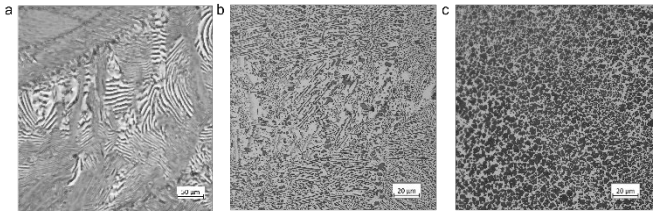

Fig. 3 OM images showing the morphology of (a) EHEA; (b) EHEA-Ti0.15, and (c) EHEA- Ti0.3.

Figure 4 showcases representative stress-strain curves for Laser Energy Net Shaped (LENS) samples possessing diverse Ti content

values. Notably, the sample with a Ti content of 0.15 atomic percent manifests an exceptional blend of strength and ductility, featuring a yield strength of 1001 MPa, an ultimate tensile strength of 1430 MPa, and an elongation of 8%. This achievement underscores an augmentation in strength alongside a minor trade-off in ductility in comparison to the Ti0.15-EHEA counterpart. With a further elevation of Ti content to 0.3 atomic percent, the ultimate tensile strength can attain 1450 MPa; however, this increment is met with a decrease in ductility. These findings indicate that diverse Ti content levels engender distinct properties within the LENS-fabricated AlCoCrFeNi2.1 EHEA.

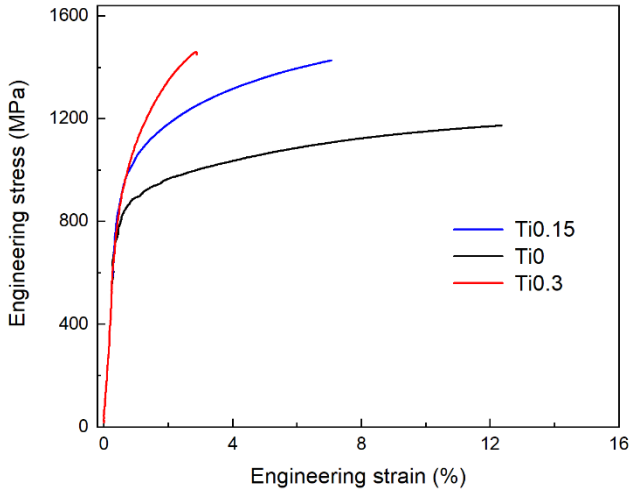

Fig. 4 Room temperature tensile stress-strain curves of EHEA, Ti0.15-EHEA, and Ti0.3-EHEA samples.

Figure 5 presents the fracture morphology of Laser Energy Net Shaped (LENS) AlCoCrFeNi2.1 alloy doped with varying Ti content levels. In order to gain deeper insights into the interplay between mechanical properties, microstructural attributes, and the fracture mechanisms of LENS-fabricated Ti-rich Eutectic High-Entropy Alloys (Tix-EHEA), scanning electron microscopy (SEM) analyses were conducted on the fracture surfaces. Distinct fracture modes emerge with varying Ti content: ductile fracture, cleavage fracture, and brittle fracture. In the absence of Ti content, the fracture surface exhibits a prevalence of fine dimples and trench-like patterns. Upon introducing Ti content up to 0.15 atomic percent, the fracture surface undergoes a noticeable transformation, revealing a substantial presence of cleavage steps alongside minor dimples. Notably, the dimple size increases, indicating a pronounced shift towards cleavage fracture as the primary mode. Upon further elevating the Ti content to 0.3 atomic percent, a pivotal transition occurs in the dominant fracture mechanism, transitioning from cleavage fracture to brittle fracture. This transition is characterized by the emergence of a fracture morphology resembling 'rock-sugar' formations.

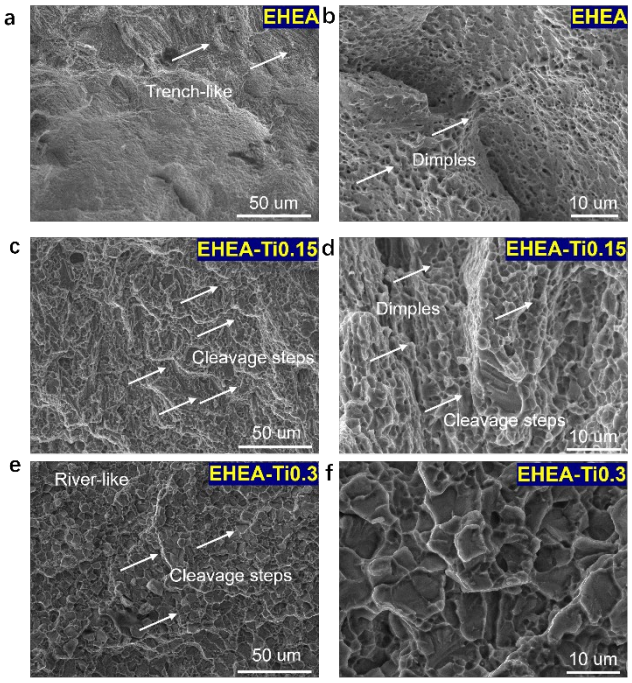

Fig. 5 The fracture morphology of the different Tix-EHEA fabricated by LENS-ed at 50 J/mm, EHEA (a)(b); EHEA-Ti0.15 (c)(d); EHEA-Ti0.3 (e)(f).

4. Conclusions

In this study, Laser Energy Net Shaping (LENS) was applied to craft Eutectic High-Entropy Alloys (EHEAs) in the Tix-AlCoCrFeNi2.1 system, aiming for a comprehensive examination of their microstructural traits and inherent attributes. Methodical variation of processing parameters led to the successful fabrication of a near-fully dense Tix-EHEA, boasting an impressive density of 99.8%, achieved through meticulous parameter optimization. Significantly, the eutectic morphology underwent a remarkable progression from lamellar structures to rod-like configurations, culminating in petal-like formations with increased Ti content. Laser Energy Net Shaped AlCoCrFeNi2.1 alloys displayed finely dispersed grains, averaging 2 μm, a result of rapid solidification dynamics. Tensile tests uncovered a compelling interplay of high strength and ductility in the LENS-formed specimens, owing to the fine grains and hierarchical structure. Remarkably, the Ti0.15-AlCoCrFeNi2.1 EHEA, produced via LENS without additional treatments, exhibited exceptional yield strengths, ultimate tensile strength, and ductility values of 1430 MPa and 8%, respectively.

ACKNOWLEDGEMENT

The work described in this paper was mainly supported by the research studentship from the Research and Innovation Office of The Hong Kong Polytechnic University (Project codes: RJHP, BBR5 and BBX2), and the Shenzhen-Hong Kong-Macau Technology Research Programme (Project No: SGDX20220530110804030). Also, we gratefully acknowledge support from the Australian Research Council (DP180103205, DP220103407, DP200100940, DP200102666, DP190102243 and IC180100005), the Australia–US Multidisciplinary University Research Initiative programme supported by the Australian Government through the Department of Defence under the Next

Generation Technologies Fund, the Research Committee of The Hong Kong Polytechnic University (PolyU) (Project code: CD4F and UAMT). The authors would also like to express their sincerely thanks to the funding support from the State Key Laboratories in Hong Kong from the Innovation and Technology Commission (ITC) of the Government of the Hong Kong Special Administrative Region (HKSAR), China.

REFERENCES

[1] Zhang W, Zhang Y. Science and technology in high-entropy alloys[J]. Science China Earth Science, 2018:2-22. Science, 2018, 362: 1925

[2] Zhao C., Zhou H., Lu Q., et al. Extra strengthening and work hardening in gradient nano twinned metals[J]. Science, 2018, 362: 1925.

[3] Yeh J W , Chen S K , Lin S J , et al. Nanostructured High-Entropy Alloys with Multiple Principal Elements: Novel Alloy Design Concepts and Outcomes[J]. Advanced Engineering Materials, 2004(5):6.

[4] Lu Y , Dong Y , Guo S , et al. A Promising New Class of High-Temperature Alloys: Eutectic High-Entropy Alloys[J]. Rep, 2014, 4:6200.

[5] Guo Y, Su H, Zhou H, et al. Unique strength-ductility balance of AlCoCrFeNi2.1 eutectic high entropy alloy with ultra-fine duplex microstructure prepared by selective laser melting [J]. Journal of Materials Science & Technology,.111 (2022) 298–306.

[6] Gu D., Hagedorn Y., Meiners W., et al. Densification behavi or, microstructure evolution, and wear performance of selective l aser melting processed commercially pure titanium. [J]. Acta Ma terialia, 2012, 60, 3849–3860.

[7] Chen X., Kong J., Li J., et al. High-strength AlCoCrFeNi2.1 eutectic high entropy alloy with ultrafine lamella structure via additive manufacturing. [J]. Materials Science & Engineering A, 2022, 854, 143816.